

# IRS-Assisted Active Device Detection

Friedemann Laue<sup>\*†</sup>, Vahid Jamali<sup>\*</sup>, and Robert Schober<sup>\*</sup>

<sup>\*</sup>Friedrich-Alexander University Erlangen-Nürnberg (FAU), <sup>†</sup>Fraunhofer IIS

**Abstract**—This paper studies intelligent reflecting surface (IRS) assisted active device detection. Since the locations of the devices are a priori unknown, optimal IRS beam alignment is not possible and a worst-case design for a given coverage area is developed. To this end, we propose a generalized likelihood ratio test (GLRT) detection scheme and an IRS phase-shift design that minimizes the worst-case probability of misdetection. In addition to the proposed optimization-based phase-shift design, we consider two alternative suboptimal designs based on closed-form expressions for the IRS phase shifts. Our performance analysis establishes the superiority of the optimization-based design, especially for large coverage areas. Furthermore, we investigate the impact of scatterers on the proposed line-of-sight based design using simulations.

## I. INTRODUCTION

Intelligent reflecting surfaces (IRSs) have gained significant attention due to their capability of transforming the wireless channel into a programmable smart radio environment [1]. An IRS comprises a large number of unit cells, which are configured to induce specific phase shifts to an impinging electromagnetic wave. Given an optimized phase-shift design for the unit cells, an IRS can significantly improve the performance of the communication system [2]. However, most works in the literature propose phase-shift designs for an active communication link and do not consider use cases where the activity and the location of a device are a priori unknown. The detection of active devices is needed, e.g., in Internet of Things (IoT) networks, where sensors provide sporadic status reports, and in the initial access stage of cellular communication systems [3], [4]. For such applications, since no communication link exists prior to the successful detection of the active devices, the phase-shift designs proposed in the literature are not applicable. Consequently, alternative phase-shift designs are required that provide basic connectivity over an IRS-assisted channel at any time and regardless of the devices' locations.

To this end, this paper studies the detection of active devices in IRS-assisted communication systems. We assume a given coverage area, where devices sporadically access the base station (BS) for data transfer by transmitting known synchronization signals, while the exact locations of the active devices are unknown. Furthermore, we assume that the direct link between the devices and the BS is blocked and an IRS is deployed to achieve connectivity. In order to find suitable phase-shift designs for the IRS, we first derive a generalized likelihood ratio test (GLRT) detector for the synchronization signals based on a physics-based model of the IRS-assisted end-to-end channel. Subsequently, we propose an optimized phase-shift design that minimizes the probability of misdetection for the devices' worst-case locations. Moreover, we study two heuristic analytical phase-shift designs and compare their

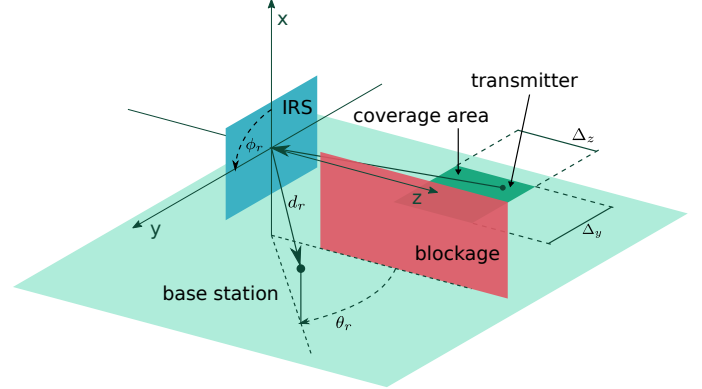


Fig. 1. Schematic illustration of the considered IRS-assisted communication setup for active device detection.

performance to that of the optimized design for various channel conditions.

We note that phase-shift optimization has also been studied for the initial access in millimeter-wave communication networks [3]–[5]. However, these results synthesize the beam pattern for a BS for specific angles whereas the IRS phase-shift design has to create a reflection pattern that depends on both the incident and the reflection directions. Thus, the results for millimeter-wave communication networks are not directly applicable to IRS-assisted systems.

*Notations:*  $\text{tr}(\mathbf{X})$ ,  $\mathbf{X}^T$ ,  $\mathbf{X}^H$ , and  $\text{diag}(\mathbf{X})$  denote the trace, transpose, conjugate transpose, and the vector comprising the elements on the main diagonal of matrix  $\mathbf{X}$ , respectively. A positive semidefinite matrix  $\mathbf{X}$  is characterized by  $\mathbf{X} \succeq 0$  and the identity matrix of size  $N \times N$  is denoted by  $\mathbf{I}_N$ .  $[\mathbf{x}]_n$  refers to the  $n$ th element of vector  $\mathbf{x}$ .  $\mathbb{R}$  and  $\mathbb{C}$  denote the set of real and complex numbers, respectively.  $\mathbf{x} \sim \mathcal{N}(\mathbf{a}, \mathbf{B})$  and  $\mathbf{x} \sim \mathcal{CN}(\mathbf{a}, \mathbf{B})$  refer to normal and complex normal distributed random vectors  $\mathbf{x}$  with mean vector  $\mathbf{a}$  and covariance matrix  $\mathbf{B}$ , respectively. The remainder of the division  $a/b$  is denoted by  $a \pmod{b}$  and the largest integer less or equal to  $x$  is given by  $\lfloor x \rfloor$ .

## II. SYSTEM MODEL

Fig. 1 illustrates the considered communication scenario consisting of a BS, an IRS, and a coverage area where the devices of interest are located. The blockage prevents a direct link between the devices and the BS. Therefore, the IRS is deployed to reflect waves originating from the coverage area towards the BS. The center of the IRS is the origin of two coordinate systems. In particular, for ease of presentation, we use a standard Cartesian coordinate system  $(x, y, z)$  to

characterize the coverage area and the IRS unit-cell locations, and a spherical coordinate system  $(d, \theta, \phi)$  to characterize the location of the BS and the incident and reflection angles on the IRS, see Fig. 1.

### A. Coverage Area and Devices

Two parameter sets define the rectangular coverage area in the  $yz$ -plane: the coordinates  $(c_x, c_y, c_z)$  of the center of the area and dimensions  $(\Delta_y, \Delta_z)$  along the  $y$  and  $z$  axes. In general, we use the coordinates  $(q_x, q_y, q_z)$  to refer to a specific location  $q$  in the coverage area, where  $q_x = c_x$ ,  $q_y \in [c_y - \Delta_y/2, c_y + \Delta_y/2]$ , and  $q_z \in [c_z - \Delta_z/2, c_z + \Delta_z/2]$ . Most of the time, a device in the coverage area is inactive and not synchronized to the BS. When new data arrives in the transmit buffer of a device, it becomes active and attempts to access the BS by transmitting a predefined synchronization signal  $\mathbf{x} \in \mathbb{C}^S$  comprising  $S$  symbols. We define a constant transmit power  $P_x$  for each symbol and assume only one device is active at a time.

### B. Intelligent Reflecting Surface

The IRS is located in the  $xy$ -plane and comprises  $U = U_x U_y$  unit cells, where  $U_x$  ( $U_y$ ) is the number of unit cells along the  $x$ -axis ( $y$ -axis). The unit-cell spacing in  $x$ -direction ( $y$ -direction) is denoted by  $d_x$  ( $d_y$ ). We define set  $\mathcal{U} = \{0, 1, \dots, U - 1\}$  and index each unit cell by  $u \in \mathcal{U}$  or by the two-dimensional index

$$u_x = u \pmod{U_x} - U_x/2 + 1 \quad (1)$$

$$u_y = \lfloor u/U_x \rfloor - U_y/2 + 1, \quad (2)$$

where we assume that  $U_x$  and  $U_y$  are even numbers. The coordinates of the  $(u_x, u_y)$ th unit cell are given by vector  $\mathbf{c}_{u_x, u_y} = [d_x u_x \ d_y u_y \ 0]^T$ . The phase shift of the  $u$ th unit cell  $\varphi_u$  determines the  $u$ th element of phase-shift vector  $\mathbf{w} \in \mathbb{C}^U$ , i.e.,  $[\mathbf{w}]_u = e^{j\varphi_u}$ .

Following the model in [6], we assume that both the transmitter (device) and the receiver (BS) are located in the far field of the IRS. Let  $\Psi_t^{(q)} = [\theta_t^{(q)} \ \phi_t^{(q)}]^T$  and  $\Psi_r = [\theta_r \ \phi_r]^T$  denote the direction from the IRS to a transmitter at location  $q$  and to the BS, respectively. Then, the IRS response function [6]

$$g(\Psi_t^{(q)}, \Psi_r) = v(\Psi_t^{(q)}, \Psi_r) \mathbf{a}^H(\Psi_t^{(q)}, \Psi_r) \mathbf{w}, \quad (3)$$

characterizes the reflected wave observed in direction  $\Psi_r$  caused by an impinging plane wave from direction  $\Psi_t^{(q)}$ . The elements of the steering vector  $\mathbf{a}(\Psi_t^{(q)}, \Psi_r)$  in (3) are given by

$$\left[ \mathbf{a}(\Psi_t^{(q)}, \Psi_r) \right]_{u_x, u_y} = e^{-j(\mathbf{k}(\Psi_t^{(q)}) + \mathbf{k}(\Psi_r))^T \mathbf{c}_{u_x, u_y}} \quad (4)$$

and

$$\mathbf{k}(\Psi) = \frac{2\pi}{\lambda} [\sin(\theta) \cos(\phi) \ \sin(\theta) \sin(\phi) \ \cos(\theta)]^T, \quad (5)$$

where  $\lambda$  denotes the wavelength and  $\Psi$  refers to an incident direction  $\Psi_t^{(q)}$  or reflection direction  $\Psi_r$ . Furthermore,  $v(\Psi_t^{(q)}, \Psi_r)$  in (3) denotes the unit cell factor and is specified in [6, Section II.D].

### C. Channel Model

We consider single-antenna devices and a multiple-antenna BS with  $M$  antenna elements. We assume IRS and BS are deployed at sufficient height such that their line-of-sight (LoS) is much stronger than any scattered links. However, since the devices are at low heights, several scatterers may contribute to the device-IRS channel. Hence, the end-to-end channel from location  $q$  in the coverage area to the BS is modelled as

$$\mathbf{h}_q = \mathbf{h}_r \sum_{l=0}^{L-1} g(\Psi_{t,l}^{(q)}, \Psi_r) h_{t,l}^{(q)}, \quad (6)$$

where  $\mathbf{h}_r = h_r \mathbf{b}$  denotes the IRS-BS channel with  $\mathbf{b} \in \mathbb{C}$  being the BS steering vector. The  $m$ th phase shift  $\varphi_m$  of  $[\mathbf{b}]_m = e^{j\varphi_m}$  is relative to the reference phase  $\varphi_r = 2\pi d_r/\lambda$  of the IRS-BS free-space channel

$$h_r = \frac{\lambda}{4\pi d_r} e^{j\varphi_r}, \quad (7)$$

where  $d_r$  denotes the IRS-BS distance. Moreover,  $L$  in (6) denotes the number of paths in the device-IRS link and  $h_{t,l}^{(q)}$  denotes the channel coefficient of the  $l$ th path, where  $l \in \{0, 1, \dots, L - 1\}$ . The LoS channel coefficient,  $h_{t,0}^{(q)}$ , is deterministic, whereas the non-LoS channel coefficients are modelled as Rayleigh fading, i.e.,

$$h_{t,l}^{(q)} = \frac{\lambda}{4\pi d_t^{(q)}} e^{j\varphi_t^{(q)}}, \quad l = 0 \quad (8)$$

$$h_{t,l}^{(q)} \sim \mathcal{CN}\left(0, P_{l, \text{NLoS}}^{(q)}\right), \quad l \neq 0. \quad (9)$$

In (8),  $\varphi_t^{(q)} = 2\pi d_t^{(q)}/\lambda$ , where  $d_t^{(q)}$  denotes the distance between device location  $q$  and the IRS. In (9),  $P_{l, \text{NLoS}}^{(q)}$  denotes the average power of the  $l$ th scattered path. Furthermore, the incident directions  $\Psi_{t,l}^{(q)}$  for  $l \neq 0$  of the scattered waves originating from location  $q$  are modelled as random variables that are specified by a given probability distribution [7].

## III. ACTIVE DEVICE DETECTION

For the design of the detection scheme at the BS, we assume that only few scatterers exist in the device-IRS link and that the LoS path contributes most power to the received signal. This assumption is justified for systems operating in the millimeter-wave frequency bands [8]. Thus, for tractability, we design the system based on the LoS link only. However, in Section V, we will investigate the impact of scatterers in the device-IRS link on the proposed design. Assuming only the LoS link exists, the received symbols that originate from a device at location  $q$  are given by

$$\mathbf{Y}_q = h_q \mathbf{b} \mathbf{x}^T + \mathbf{Z}, \quad (10)$$

where the element in the  $m$ th row and  $s$ th column of  $\mathbf{Y}_q \in \mathbb{C}^{M \times S}$  denotes the symbol received at the  $m$ th BS antenna and in the  $s$ th symbol interval,  $s \in \{0, 1, \dots, S - 1\}$ . Moreover, the end-to-end channel coefficient is given by  $h_q = h_r g(\Psi_{t,0}^{(q)}, \Psi_r) h_{t,0}^{(q)}$  and the elements of  $\mathbf{Z} \in \mathbb{C}^{M \times S}$  are mutually independent complex normal random variables with zero mean and variance  $\sigma_n^2$ , denoting additive white Gaussian

noise. We assume  $\mathbf{b}$  is given and fixed because its values only depend on the geometry of the BS antenna. Therefore, we adopt a matched filter  $\mathbf{v}^H = \mathbf{b}^H / \sqrt{M}$  at the BS and obtain the filtered signal

$$\mathbf{y}_q^T = \mathbf{v}^H \mathbf{Y}_q = \sqrt{M} h_q \mathbf{x}^T + \mathbf{z}^T = \mathbf{s}_q^T e_q + \mathbf{z}^T, \quad (11)$$

where  $\mathbf{z}^T = \mathbf{v}^H \mathbf{Z} \sim \mathcal{CN}(0, \sigma_n^2 \mathbf{I}_S)$ ,  $\mathbf{s}_q^T = \mathbf{x}^T \sqrt{M} |h_q|$ , and  $e_q = \exp(j \arg(h_q))$ . Here,  $\arg(h_q)$  denotes the phase of  $h_q$ . Although we can determine  $e_q$  using (3), (7), and (8), its value depends on the exact knowledge of distances  $d_r$  and  $d_t^{(q)}$ . In practice, these distances have to be obtained from measurements with a limited accuracy. Unfortunately, even small deviations (on the order of wavelengths) from the exact values may result in large variations of  $\arg(h_q)$  and consequently of  $e_q$ . As a result, we model  $e_q$  as a deterministic, but unknown variable. On the other hand, the impact of estimation errors for  $d_r$  and  $d_t^{(q)}$  on  $|h_q|$  and equivalently  $\mathbf{s}_q$  is less significant. Hence, we assume that  $|h_q|$  and  $\mathbf{s}_q$  are known.

In general, for active-device detection, two hypotheses are defined and the detector decides for either of them given the observation [9]. For the problem at hand, the hypotheses are:

$$\mathcal{H}_0 : \text{device inactive} \quad \Rightarrow \mathbf{y}_q = \mathbf{z} \quad (12)$$

$$\mathcal{H}_1 : \text{device active} \quad \Rightarrow \mathbf{y}_q = \mathbf{s}_q e_q + \mathbf{z} \quad (13)$$

For derivation of the detection scheme, we apply the GLRT concept, which replaces the unknown variable  $e_p$  by its maximum likelihood estimate. Denote  $f(\mathbf{y}_q; e_q, \mathcal{H}_1)$  as the probability density function (PDF) of  $\mathbf{y}_q$  under  $\mathcal{H}_1$  with parameter  $e_q$  and  $f(\mathbf{y}_q; \mathcal{H}_0)$  as the PDF of  $\mathbf{y}_q$  under  $\mathcal{H}_0$ . Then, the generalized likelihood ratio for considered scenario is given by

$$L_G(\mathbf{y}_q) = \frac{\max_{e_q} f(\mathbf{y}_q; e_q, \mathcal{H}_1)}{f(\mathbf{y}_q; \mathcal{H}_0)} \quad (14)$$

and the detector decides for  $\mathcal{H}_1$  when (14) is larger than a detection threshold  $t'$ . For  $S > 1$ , it can be shown [9, Chapter 7] that  $L_G(\mathbf{y}_q) > t'$  is equivalent to

$$T(\mathbf{y}_q) = 2 \ln L_G(\mathbf{y}_q) = 2 \frac{|\mathbf{s}_q^H \mathbf{y}_q|^2}{\sigma_n^2 \|\mathbf{s}_q\|^2} > 2 \ln t' = t. \quad (15)$$

The distribution of  $T(\mathbf{y}_q)$  under both hypotheses is

$$\mathcal{H}_0 : T(\mathbf{y}_q) \sim \chi_2^2(0) \quad (16)$$

$$\mathcal{H}_1 : T(\mathbf{y}_q) \sim \chi_2^2(\gamma_q), \quad (17)$$

where  $\chi_2^2(\gamma_q)$  denotes a  $\chi^2$  distribution with 2 degrees of freedom and non-centrality parameter

$$\gamma_q = 2SM |h_q|^2 \frac{P_x}{\sigma_n^2}. \quad (18)$$

One can directly obtain the probability of false alarm  $\Gamma_{\text{FA}} = \Pr\{T(\mathbf{y}_q) > t | \mathcal{H}_0\}$  and the probability of misdetection  $\Gamma_{\text{MD}}^{(q)} = \Pr\{T(\mathbf{y}_q) < t | \mathcal{H}_1\}$  from (16) and (17) as [9, Chapter 13.4]

$$\Gamma_{\text{FA}} = 1 - F_{\chi_2^2(0)}(t) \quad \text{and} \quad \Gamma_{\text{MD}}^{(q)} = F_{\chi_2^2(\gamma_q)}(t), \quad (19)$$

where  $F_{\chi_2^2(\gamma_q)}(t)$  denotes the cumulative distribution function (CDF) of a  $\chi_2^2(\gamma_q)$  distribution. We observe from (19) that

for a given desired probability of false alarm, the respective detection threshold  $t$  is given by  $t = F_{\chi_2^2(0)}^{-1}(1 - \Gamma_{\text{FA}})$ .

#### IV. PHASE-SHIFT CONFIGURATION

The phase-shift vector  $\mathbf{w}$  in (3) controls the reflection of the waves impinging on the IRS. The ideal phase-shift design should provide a low misdetection probability for the entire coverage area because the location  $q$  of the active device is not a priori known. Therefore, we formulate a worst-case optimization problem for minimizing the probability of misdetection. Moreover, we propose two heuristic approaches employing closed-form phase-shift vectors.

##### A. Optimal Phase-Shift Design

We target a phase-shift design that minimizes the worst-case probability of misdetection  $\Gamma_{\text{MD}}^{(q)}$  across the entire coverage area. For tractability of the optimization problem, we model the coverage area as a set of  $Q$  locations obtained from a grid in the  $yz$ -plane. Then, every location of interest is index by  $q \in \{0, 1, \dots, Q-1\} = \mathcal{Q}$ . We note that the grid can be selected to guarantee a desired accuracy, e.g., the grid spacing can be chosen sufficiently small such that two adjacent locations experience approximately the same channel gain. The optimization objective is the minimization of the largest  $\Gamma_{\text{MD}}^{(q)}$  for  $q \in \mathcal{Q}$ . However,  $\Gamma_{\text{MD}}^{(q)}$  in (19) is a monotonically decreasing function in  $\gamma_q$  such that an equivalent objective is the maximization of the smallest  $\gamma_q$  for  $q \in \mathcal{Q}$ . Moreover, omitting the constant factors in (18), the objective reduces to maximizing the smallest

$$|h_q|^2 = \left| \frac{\lambda}{4\pi d_r} \frac{\lambda}{4\pi d_t^{(q)}} v(\Psi_t^{(q)}, \Psi_r) \mathbf{a}^H(\Psi_t^{(q)}, \Psi_r) \mathbf{w} \right|^2 \quad (20)$$

for  $q \in \mathcal{Q}$ . Using the definitions

$$\bar{\mathbf{a}}^H(\Psi_t^{(q)}, \Psi_r) = \frac{\lambda}{4\pi d_r} \frac{\lambda}{4\pi d_t^{(q)}} v(\Psi_t^{(q)}, \Psi_r) \mathbf{a}^H(\Psi_t^{(q)}, \Psi_r) \quad (21)$$

$$\bar{\mathbf{A}}(\Psi_t^{(q)}, \Psi_r) = \bar{\mathbf{a}}(\Psi_t^{(q)}, \Psi_r) \bar{\mathbf{a}}^H(\Psi_t^{(q)}, \Psi_r), \quad (22)$$

we rewrite (20) as  $|h_q|^2 = \mathbf{w}^H \bar{\mathbf{A}}(\Psi_t^{(q)}, \Psi_r) \mathbf{w}$  and formulate the following optimization problem:

$$\begin{aligned} \text{(P1)} \quad & \max_{\mathbf{w}} \min_{\forall q \in \mathcal{Q}} \mathbf{w}^H \bar{\mathbf{A}}(\Psi_t^{(q)}, \Psi_r) \mathbf{w} \\ & \text{s.t.} \quad \|\mathbf{w}\|_u = 1, \quad \forall u \in \mathcal{U} \end{aligned}$$

Problem (P1) is not convex in  $\mathbf{w}$  due to the unit-modulus constraint [10]. A common approach to obtain an approximate solution of (P1) is semi-definite relaxation (SDR) [11]. Using  $\mathbf{W} = \mathbf{w} \mathbf{w}^H$  and  $\mathbf{w}^H \bar{\mathbf{A}}(\Psi_t^{(q)}, \Psi_r) \mathbf{w} = \text{tr}(\bar{\mathbf{A}}(\Psi_t^{(q)}, \Psi_r) \mathbf{W})$ , a relaxed version of (P1) is obtained as

$$\begin{aligned} \text{(P2)} \quad & \max_{\mathbf{W}, \tau} \tau \\ & \text{s.t.} \quad \tau \leq \text{tr}(\bar{\mathbf{A}}(\Psi_t^{(q)}, \Psi_r) \mathbf{W}), \quad \forall q \in \mathcal{Q} \\ & \quad \text{diag}(\mathbf{W}) = \mathbf{1} \\ & \quad \mathbf{W} \succeq 0. \end{aligned}$$

Standard convex solvers, e.g., [12], find the optimal solution  $\mathbf{W}_{\text{opt}}$  of (P2), but  $\text{rank}(\mathbf{W}_{\text{opt}}) = 1$  cannot be guaranteed, which means we cannot obtain the optimal phase-shift vector  $\mathbf{w}_{\text{opt}}$  from  $\mathbf{W}_{\text{opt}}$  directly. Instead, we determine an approximation  $\hat{\mathbf{w}}_{\text{opt}}$  using Gaussian randomization [11]:

- 1) For  $g \in \{0, 1, \dots, G-1\} = \mathcal{G}$ , generate  $G$  random vectors  $\boldsymbol{\nu}_g \sim \mathcal{CN}(0, \mathbf{W}_{\text{opt}})$ .
- 2) For  $g \in \mathcal{G}$ , set  $|\boldsymbol{\nu}_g|_u = 1 \forall u \in \mathcal{U}$ .
- 3)  $\hat{\mathbf{w}}_{\text{opt}} = \arg \max_{\boldsymbol{\nu}_g, \forall g \in \mathcal{G}} \min_{\forall q \in \mathcal{Q}} \boldsymbol{\nu}_g^H \bar{\mathbf{A}}(\boldsymbol{\Psi}_t^{(q)}, \boldsymbol{\Psi}_r) \boldsymbol{\nu}_g$ .

In the remainder of this work, we refer to  $\hat{\mathbf{w}}_{\text{opt}}$  as the optimized phase-shift design. Problem (P2) is a semi-definite programming problem and, given a solution accuracy  $\epsilon > 0$ , can be solved with a worst-case computational complexity of  $\mathcal{O}((U+Q)^4 \sqrt{U} \log(1/\epsilon))$  [11]. Although there is a polynomial dependency on  $U$  and  $Q$ , the complexity can be afforded because the considered phase-shift design is an offline problem that is solved once in the design stage of the system. Nevertheless, in the next subsection, we propose two closed-form phase-shift designs that entail a lower complexity than the optimized design.

### B. Heuristic Phase-Shift Designs

In the following, we consider analytical phase-shift vector designs characterized by

$$[\mathbf{w}]_{u_x, u_y} = \exp(j [u_x \quad u_y \quad 0] \nabla \omega(u_x, u_y)), \quad (23)$$

where  $\nabla \omega(u_x, u_y) \in \mathbb{R}^3$  denotes the phase-shift gradient.

The first design is based on a constant phase gradient that results in a linear phase-shift design. It is known that such a design maximizes the reflection gain for a specific incident direction [6]. A straightforward approach chooses the center of the coverage area as the direction for maximum gain, but this leads to poor performance at the corners of the area. Therefore, we propose a design that partitions the IRS and the coverage area into  $K$  tiles, respectively, indexed by  $k \in \{0, 1, \dots, K-1\} = \mathcal{K}$ . Then, we apply the linear phase-shift design where each tile of the IRS covers one tile of the coverage area. The partitioning is performed along the  $y$ -axis and the  $k$ th tile of the IRS is specified by  $u_y^{(k)} \in \{kU_y/K - U_y/2 + 1, \dots, (k+1)U_y/K - U_y/2\}$ . Furthermore,  $\boldsymbol{\Psi}_t^{(c_k)}$  denotes the direction from the IRS to the center of the  $k$ th tile of the coverage area. This results in the phase gradient

$$\nabla \omega(u_x, u_y^{(k)}) = - \left( \mathbf{k}(\boldsymbol{\Psi}_t^{(c_k)}) + \mathbf{k}(\boldsymbol{\Psi}_r) \right) \quad (24)$$

and specifies the phase-shift vector of the  $k$ th tile.

The second design is based on the work in [13], which uses a linear phase-shift gradient resulting in a quadratic phase-shift design. This approach provides wide coverage by design. The main idea is to determine the required constant phase gradients for every location of the coverage area and obtain their minimum and maximum values. Then, the phase gradient interpolates between these values with a linear function to cover to entire area. To this end, we define the phase gradient

$$\nabla \omega(u_x, u_y) = \begin{bmatrix} u_x & 0 & 0 \\ 0 & u_y & 0 \\ 0 & 0 & 0 \end{bmatrix} \begin{bmatrix} \alpha_x \\ \alpha_y \\ 0 \end{bmatrix} + \begin{bmatrix} \beta_x \\ \beta_y \\ 0 \end{bmatrix} \quad (25)$$

TABLE I  
SIMULATION PARAMETERS

Parameter	Value	Parameter	Value
$\lambda$	0.1 m	$(d_x, d_y)$	$(\lambda/2, \lambda/2)$
$(U_x, U_y)$	(8, 8)	$(c_x, c_y, c_z)$	(-10 m, -50 m, 50 m)
$(d_r, \theta_r, \phi_r)$	(30 m, 0°, 90°)	$M$	16
$\Gamma_{\text{FA}}$	0.1	$P_x$	28 dBm
$\sigma_n^2$	-95 dBm	$S$	32

and determine  $\alpha_x$ ,  $\alpha_y$ ,  $\beta_x$ , and  $\beta_y$  by solving

$$\begin{aligned} \nabla \omega(u_x^{\min}, u_y^{\min}) &= \min_{\forall q \in \mathcal{Q}} - \left( \mathbf{k}(\boldsymbol{\Psi}_t^{(q)}) + \mathbf{k}(\boldsymbol{\Psi}_r) \right) \\ \nabla \omega(u_x^{\max}, u_y^{\max}) &= \max_{\forall q \in \mathcal{Q}} - \left( \mathbf{k}(\boldsymbol{\Psi}_t^{(q)}) + \mathbf{k}(\boldsymbol{\Psi}_r) \right), \end{aligned} \quad (26)$$

where the min and max operations are elementwise and  $u_x^{\min} = -U_x/2 + 1$ ,  $u_y^{\min} = -U_y/2 + 1$ ,  $u_x^{\max} = U_x/2$ , and  $u_y^{\max} = U_y/2$ . Thus, (25) and (26) specify the phase-shift vector in (23).

## V. PERFORMANCE RESULTS

In this section, we study the misdetection probability for the proposed phase-shift designs. We set the noise power as  $\sigma_n^2 = N_0 B F = -95$  dBm assuming noise power spectral density (PSD)  $N_0 = -174$  dBm/Hz, signal bandwidth  $B = 20$  MHz, and noise figure  $F = 6$  dB. Table I specifies all relevant system parameters.

To illustrate the impact of different phase-shift designs on the reflection beams of the IRS, Fig. 2 shows the misdetection probability for all points in the  $yz$ -plane with  $x = -10$  m, i.e., at the ground. The beam of the linear design with  $K = 1$  is focused at the center of the coverage area and does not provide sufficient gain in the upper right corner of the area. The quadratic design generates a well aligned beam. However, compared to the optimized design, it is not wide enough to create high gain for the entire coverage area.

Fig. 3 shows the maximum misdetection probability  $\Gamma_{\text{MD}} = \max_{q \in \mathcal{Q}} \Gamma_{\text{MD}}^{(q)}$  based on (19) for the LoS case, i.e.,  $L = 1$ . We plot  $\Gamma_{\text{MD}}$  for the heuristic designs using the analytical phase-shift vector in (23) whereas the curve for the optimized design represents the average  $\Gamma_{\text{MD}}$  obtained for 80 randomized phase-shift vectors  $\hat{\mathbf{w}}_{\text{opt}}$  with  $G = 3000$ . We observe that the optimized design provides the best performance. The heuristic designs achieve similar results for small areas, but cannot compete with the optimized design for larger areas. Moreover, for large areas, the linear design with  $K = 4$  outperforms the design with  $K = 1$ , which confirms that larger areas require a wider reflection beam, i.e., more tiles. This is inherently taken into account by the quadratic design, which yields a better performance than both linear designs for all considered sizes of the coverage area.

The impact of scatterers in the device-IRS link on the proposed LoS-based design is shown in Fig. 4. We set  $L = 5$  and  $P_{i, \text{NLoS}}^{(q)} = \frac{\rho}{L-1} |h_{t,0}^{(q)}|^2$ , where we vary  $\rho$  to evaluate different scattering conditions. The scatterers' locations are in the local environment of the active device and their incident

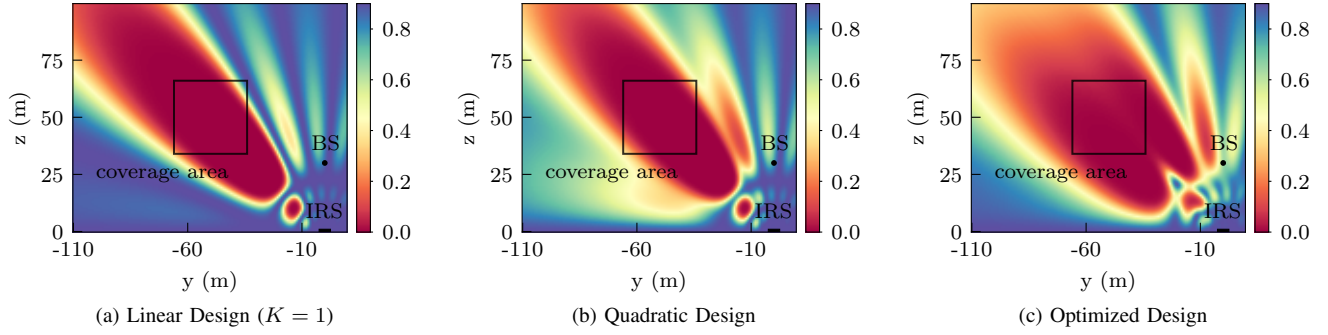


Fig. 2. Misdetection probability for different phase-shift designs and area side length  $\Delta_y = \Delta_z = 30$  m.

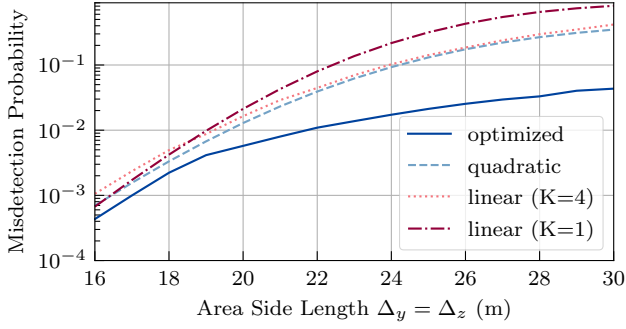


Fig. 3. Phase-shift design comparison for LoS channels.

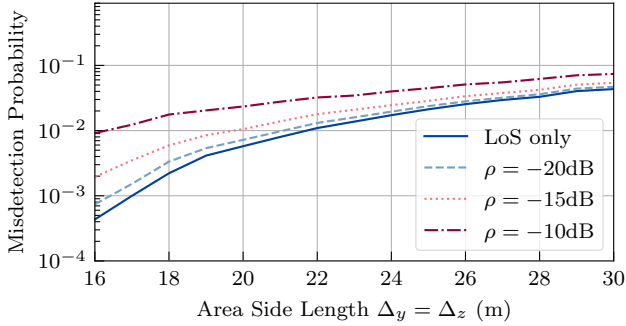


Fig. 4. Optimized phase-shift design with scattered device-IRS channel.

directions are chosen as  $\Psi_{t,l>0}^{(q)} \sim \mathcal{N}(\Psi_{t,0}^{(q)}, \text{diag}(0.1^2, 0.1^2))$ . Fig. 4 shows the average worst-case misdetection probability obtained from Monte-Carlo simulations evaluating (15). In the presence of scatterers, we observe an increase of  $\Gamma_{\text{MD}}$  compared to the LoS case because the non-LoS components in (6) may add up destructively, leading to fading and a lower received power. The variation of the received power has less impact on  $\Gamma_{\text{MD}}$  when the size of the area is large, as in this case, the size of the coverage area is the performance limiting factor.

## VI. CONCLUSION

This paper studied active device detection in an IRS-assisted communication system. We derived a GLRT detector and an optimized worst-case phase-shift design for a given coverage area. Besides, we proposed two heuristic phase-shift designs.

Our performance comparison showed the superiority of the optimized design and demonstrated the impact of scattering on the LoS-based designs. More sophisticated phase-shift designs that take into account the impact of scattering constitute an interesting topic for future work.

## REFERENCES

- [1] Renzo *et al.*, "Smart radio environments empowered by reconfigurable intelligent surfaces: How it works, state of research, and the road ahead," *IEEE J. Sel. Areas Commun.*, vol. 38, pp. 2450–2525, Jul. 2020.
- [2] Wu and Zhang, "Intelligent reflecting surface enhanced wireless network via joint active and passive beamforming," *IEEE Trans. Wireless Commun.*, vol. 18, pp. 5394–5409, Nov. 2019.
- [3] Habib *et al.*, "Millimeter wave cell search for initial access: Analysis, design, and implementation," in *13th International Wireless Communications and Mobile Computing Conference (IWCMC)*, 2017.
- [4] Yan and Cabric, "Compressive initial access and beamforming training for millimeter-wave cellular systems," *IEEE Journal of Selected Topics in Signal Processing*, vol. 13, pp. 1151–1166, Jul. 2019.
- [5] Aykin and Krunz, "Efficient beam sweeping algorithms and initial access protocols for millimeter-wave networks," *IEEE Trans. Wireless Commun.*, vol. 19, pp. 2504–2514, Jan. 2020.
- [6] Najafi *et al.*, "Physics-based modeling and scalable optimization of large intelligent reflecting surfaces," *IEEE Trans. Commun.*, vol. 69, pp. 2673–2691, Dec. 2020.
- [7] Bjornson and Sanguinetti, "Rayleigh fading modeling and channel hardening for reconfigurable intelligent surfaces," *IEEE Commun. Lett.*, pp. 830–834, Dec. 2020.
- [8] Rappaport *et al.*, "Broadband millimeter-wave propagation measurements and models using adaptive-beam antennas for outdoor urban cellular communications," *IEEE Trans. Antennas Propag.*, vol. 61, pp. 1850–1859, Dec. 2012.
- [9] Kay, *Fundamentals of Statistical Signal Processing, Volume II: Detection Theory*. Prentice Hall, 1998.
- [10] Zhang and Huang, "Complex quadratic optimization and semidefinite programming," *SIAM Journal on Optimization*, vol. 16, pp. 871–890, Jan. 2006.
- [11] Luo *et al.*, "Semidefinite relaxation of quadratic optimization problems," *IEEE Signal Process. Mag.*, vol. 27, pp. 20–34, May 2010.
- [12] ApS, *Introducing the MOSEK Optimization Suite 9.2.*, 2021. [Online]. Available: <https://docs.mosek.com/9.2/intro/index.html>
- [13] Jamali *et al.*, "Power efficiency, overhead, and complexity tradeoff of IRS codebook design – quadratic phase-shift profile," *IEEE Commun. Lett.*, Feb 2021.